International Journal of Power Electronics and Drive System (IJPEDS)
Vol. 17, No. 3, September 2026, pp. 1564~1580
ISSN: 2088-8694, DOI: 10.11591/ijpeds.v17.i3.pp1564-1580

Hybrid active filter control for harmonic reduction in quadratic boost converter-integrated grid systems

S. Venkata Ramana Rao, Mahiban Lindsay
Department of Electrical and Electronics Engineering, Hindustan University, Chennai, India

Article Info

Article history:

Received Nov 24, 2025
Revised Jul 30, 2026
Accepted Aug 14, 2026

Keywords:

Fractional-order proportional-integral-derivative
Hybrid active filter
Power quality
Quadratic boost converter
Total harmonic distortion

ABSTRACT

This article examines the proportional-integral (PI) and fractional-order proportional-integral-derivative (FOPID) controllers for a quasi-buck converter-hybrid active filter (QBC-HAF) to improve the harmonic suppression and power quality of a hybrid energy storage system (HESS) fed to the grid. This system uses a high-gain QBC, which is connected to a VSI to control the DC-link voltage and to allow controlled energy transfer from photovoltaic and battery sources. A MATLAB/Simulink test bed and hardware prototype were developed to validate performance. The results demonstrate the enhanced stability and quality of the output waveforms for both controllers, with the FOPID providing better harmonic suppression, reducing output current total harmonic distortion (THD) from 4.34% to 4.14% and output voltage THD from 4.75% to 4.42%. The simulation results were validated using experimental tests, showing that the FOPID-controlled QBC-HAF system is suitable for power quality improvement, voltage stabilization, and dynamic performance in renewable integrated grids.

Corresponding Author:

S. Venkata Ramana Rao
Department of Electrical and Electronics Engineering, Hindustan University
Rajiv Gandhi Salai, OMR, Padur, Chennai, Tamil Nadu, India
Email: vramanor@hindustanuniv.ac.in

1. INTRODUCTION

Power networks are now decentralized and dynamic power systems, as modern power grids increasingly accommodate renewable energy generation, including photovoltaic (PV) systems, in the grid. However, photovoltaic systems have faced a lot of challenges in connecting to grid networks, such as voltage instability, loss of power quality, harmonics, and much more. To overcome these issues, advanced maximum power point tracking methods have been suggested, and some comparative analyses have been performed; for instance, adaptive neuro-fuzzy inference system (ANFIS) and incremental conductance (IC) are found to be effective methods in suppressing harmonic distortion within a grid-tied photovoltaic power system [1]. The operation of current source inverter (CSI) and voltage source inverter (VSI) in parallel, for system reliability and improvement of the system efficiency, has also been studied [2]. Due to the intermittency of renewables and the requirement to incorporate renewable energy with the grid, a hybrid energy storage system (HESS) has been developed as an approach [3]. New developments have shown the viability of integrating batteries and supercapacitors for longer operations in nanosatellite applications [4], [5]. Moreover, fractional-order controllers have been extensively used for stabilizing several areas of power systems with renewable energy generation in solar plants [6], solar trackers [7], and hybrid power filters [8]. Nonlinear fractional-order proportional–integral (NFOPI) controllers have also been reported to provide better sustainable energy management for hybrid systems [9].

Harmonic reduction techniques for cascaded multilevel inverter distributed systems for renewable energy have been well studied [10] and are discussed in this paper. Innovations in the converter, such as the high-gain quadratic boost converter, which offers improved efficiency and voltage regulation, are present [11]. An optimization-based fractional-order proportional–integral–derivative (FOPID) controller has been employed to achieve power factor correction and rectification in power converters [12], and a hybrid fuzzy-seismic control framework has been applied to improve dynamic stability [13].

The wind energy system is a case study where optimal tuning of the FOPID controller is done by using golden eagle optimization [14]. The study presented a distribution static synchronous compensator (DSTATCOM) and hybrid active power filter (HAPF)-based approach for reducing total harmonic distortion (THD) and regulating the voltage in power distribution systems, demonstrating improved power quality and voltage control performance. [15]. There has been a wide range of applications of unified power quality conditioners to improve the performance of a microgrid [16], and modular multilevel inverter topologies have been proposed for improving the integration of PV [17]. The conventional and dual unified power quality conditioner (UPQC) systems have been modeled using small-signal analysis, which led to a detailed evaluation of the overall system performance [18], and dual unified power quality conditioner–photovoltaic (UPQC–PV) systems with no direct current (DC)-link capacitors have been modeled using fuzzy-Sugeno methods [19].

Stand-alone hydropower systems have also been addressed with the development of UPQC strategies that are based on observers [20]. However, more comprehensive assessments of microgrid technologies highlight the need to address power quality issues for reliable operation [21], renewable-integrated UAPF-fed microgrids were proposed to be effective in power flow management [22]. Case studies also illustrate the vital importance of power quality in today's power systems [23]. Artificial Intelligence-based approaches, such as an artificial neural network (ANN) controller-based UPQC system, have been seen as a great method to improve the overall performance of PV-integrated power system distribution networks [24]. Jellyfish search and particle swarm optimization algorithms have been proposed to tune a FOPID controller for power quality conditioners [25].

These studies emphasize the importance of creative designs of converters, synergies between hybrid storage systems and intelligent control systems to promote effective, reliable, and sustainable operation of renewable energy systems. From the literature, the research gap was identified, and the novelty of the proposed work. Previous studies investigated either quasi-buck converters (QBCs) or hybrid active filters (HAFs) independently; this work presents an integrated QBC–HAF configuration regulated by PI and FOPID controllers for simultaneous voltage regulation and harmonic reduction in grid-connected renewable energy sources (RES). The proposed system provides improved transient response and superior harmonic mitigation compared with the conventional PI controller.

The HAF is an effective solution for current and voltage harmonics caused by non-linear loads. This technology helps to dynamically improve power factor across the hybrid power system. This makes the system effective for reactive power compensation. In addition to harmonics, the filter serves multiple grid stability uses. These include dampening resonance that could otherwise stress equipment and destabilize the grid. Compared to conventional filtering systems, this design better avoids wasting energy, maintaining a more reliable supply of active power. The filter's ability to smooth peak voltage makes the overall power system more resilient by shrinking the steady-state error with peaks. This steady-state control at the point of common coupling helps integrate large amounts of modern renewable energy resources.

Modern industrial power grids are increasingly experiencing various nonlinear loads like variable speed drives (VSDs), light-emitting diode (LED) lighting systems, and computer equipment. These devices cause large harmonic currents that result in waveform distortion of voltage and current. Such harmonics can cause transformers to overheat, trip circuit breakers more frequently, and cause increased ageing of electrical equipment. Distorted power signals are especially harmful to sensitive electronic devices and may cause them to malfunction or even be permanently destroyed. In addition to equipment stress, harmonics have other effects on overall system efficiency, such as increased reactive power demand and instability of renewable energy systems connected to the grid. To overcome these issues, HAFs are used to minimize harmonics, enhance the power factor, and keep the industrial power network in stable operation by performing both passive and active filtering.

Although previous research has investigated DC–DC converters with maximum voltage gain and HAF for utilization of renewable energy technologies, limited attention has been given to the coordinated integration of a QBC with an HAF under advanced closed-loop control. Existing works mainly focus on converter voltage boosting or harmonic mitigation separately, while comprehensive studies combining both objectives are scarce. Moreover, comparative investigations between PI and FOPID controllers for QBC–HAF systems have not been adequately reported.

2. SYSTEM DESCRIPTION

2.1. Block diagram of the PI/FOPID closed-loop control system

The proposed block diagram of the QBC-fed HAF system in Figure 1 is modeled in closed loop to regulate the converter output voltage. The PI controller regulates the output voltage to track its reference using proportional and integral actions, while the FOPID controller adds fractional-order terms for better flexibility in shaping the transient response and accuracy. Both controllers use DC-link voltage feedback to generate switching signals for the converter, ensuring effective harmonic suppression and improved power quality.

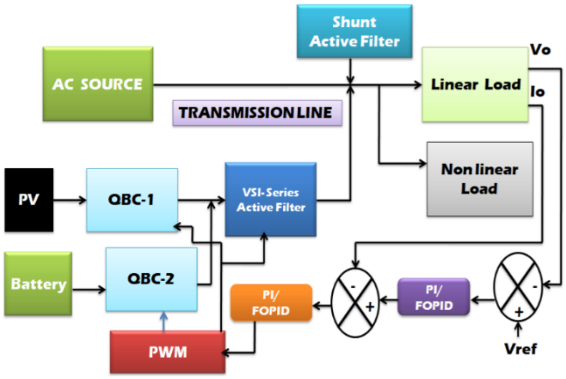

Figure 1. Block diagram of the PI/FOPID closed-loop control system

2.2. Circuit schematic of the closed-loop PI/FOPID control system

Figure 2 shows the circuit schematic of the closed-loop PI/FOPID system. In this configuration, the controller constantly monitors the variation of the actual system response from the reference input. According to this error, the controller tweaks the control signal to ensure the system output moves towards the pre-set value. This feedback mechanism helps maintain accuracy and stability in the overall system performance.

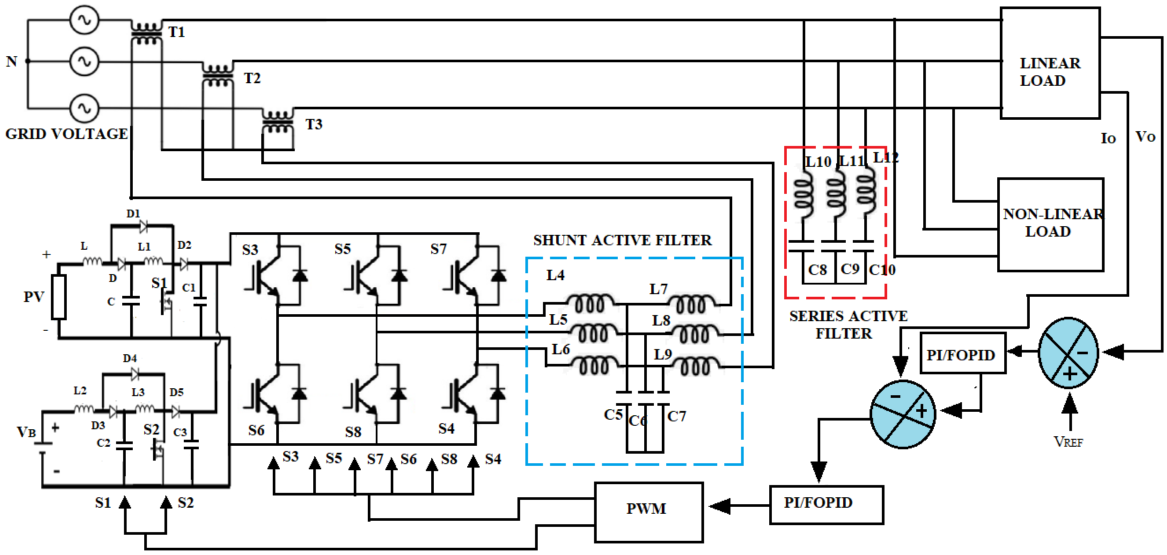

Figure 2. Circuit schematic of the closed-loop PI/FOPID control system

2.3. Circuit schematic of QBC

Figure 3 shows the developed QBC with a high-gain, step-up converter targeting renewable energy systems that require large voltage boosts. The proposed QBC topology consists of a single primary switching metal-oxide-semiconductor field-effect transistor (MOSFET) (M1), comprising a dual-inductor, dual-capacitor, and three-diode configuration. The duty cycle, denoted by (K), governs the conduction interval of the switch and consequently influences the voltage conversion ratio. The QBC, operating in uninterrupted conduction mode, offers a square-wave voltage transformation ratio, providing significantly increased conversion gain relative to conventional boost converters. This feature of the QBC makes it highly useful for battery-integrated and photovoltaic hybrid energy systems that require a reliable elevated voltage DC link for grid interfacing. The operation of the proposed converter toggles between two distinct modes based on the state of the MOSFET switch. The first mode, with the MOSFET switch in the on state, enables the inductors to charge while the capacitors discharge to the load. In the second mode, the on state of the switch is reversed, and the inductors release their stored energy through the diodes to supply the load and charge the capacitors. The proposed QBC circuit is compact and ideal for integration with other components.

2.3.1. First operating mode of QBC

Figure 4 illustrates the operation of the proposed QBC during the first operating mode. When the main switch M1 is energized, diodes D1 and D3 become reverse-biased, while diode D2 conducts. Throughout this interval, inductor L1 stores energy supplied by the input source. Whereas energy is stored in inductor L2 by capacitor C1. Simultaneously, the load is supplied by capacitor C2, resulting in a slight decrease in its voltage.

$$(\Delta IL1)\ On = \frac{V_S K_T}{L_1} \quad (1)$$

$$(\Delta IL2)\ On = \frac{V_{SKT}}{L_1} \quad (2)$$

The currents flowing through the capacitors are given by (3) and (4).

$$(IC1)\ On = -IL2 \quad (3)$$

$$(IC2)\ On = -I0 \quad (4)$$

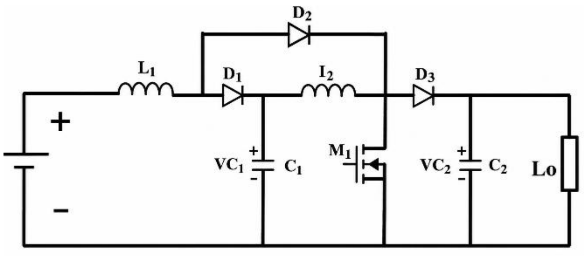

Figure 3. Circuit schematic of QBC

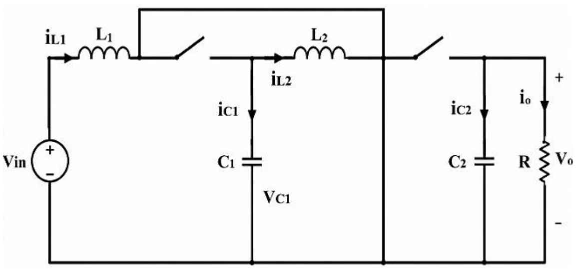

Figure 4. QBC topology during SW switch conduction

2.3.2. Second operating mode of QBC

Figure 5 illustrates the operation of the proposed QBC during the second operating mode. When the M1 switch is turned off, the energy stored in the inductors is transferred through diodes D1 and D3 to capacitors C1 and C2 and the load. Inductor L1 transfers energy to L2, whereas L2 supplies power directly to the load. During this interval, both capacitors are charged, while the inductor voltages reverse polarity as the inductor currents decrease.

$$(\Delta IL1)\ Off = \frac{V_S - V_{C1}(1-K)T}{L_1} \quad (5)$$

$$(\Delta IL2)\ Off = \frac{V_{C1} - V_0(1-K)T}{L_2} \quad (6)$$

The converter efficiency is evaluated as (7).

$$\eta = \frac{P_{out}}{P_{in}} \times 100\% \quad (7)$$

Where Ploss = P_{MOSFET} + P_{Diode} + P_{Inductor} + P_{Capacitor}. The manuscript now discusses conduction and switching losses of the MOSFET together with diode conduction losses and passive component losses. The estimated converter efficiency is approximately 95–97%, demonstrating suitability for renewable-energy applications.

- Justification with appropriate design calculations

The voltage output corresponds to the high-gain DC-link voltage produced by the QBC and not the grid RMS voltage. The reported voltage corresponds to the converter DC-link voltage obtained using the high-gain quadratic boost topology. The converter voltage gains are as in (8), where D denotes the duty ratio.

$$M = \frac{V_O}{V_{in}} = \frac{1}{(1-D)^2} \quad (8)$$

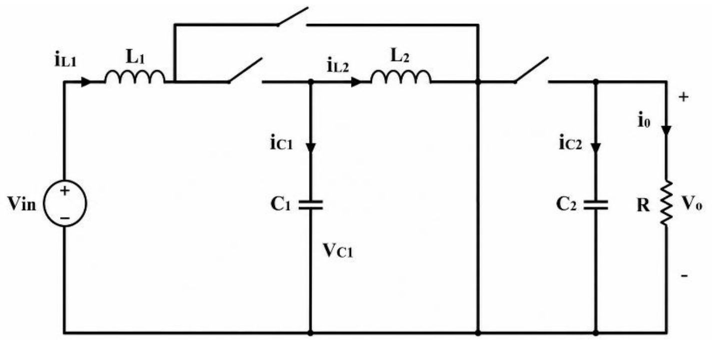

Figure 5. QBC topology during switch SW non-conduction

3. SIMULATED PERFORMANCE ANALYSIS
3.1. System schematic of QBC-HAF using a PI controller in MATLAB/Simulink

Figure 6 shows the configuration of the QBC-HAF controlled by a closed-loop PI control scheme. This controller regulates the switching action to maintain a stable high-gain output even during load-side or supply-side variations. The quadratic boost converter with HAF, with closed-loop controlled simulation specifications are given in Table 1. The table includes the controller gains, passive component values, semiconductor device ratings, and load resistance employed in the proposed configuration.

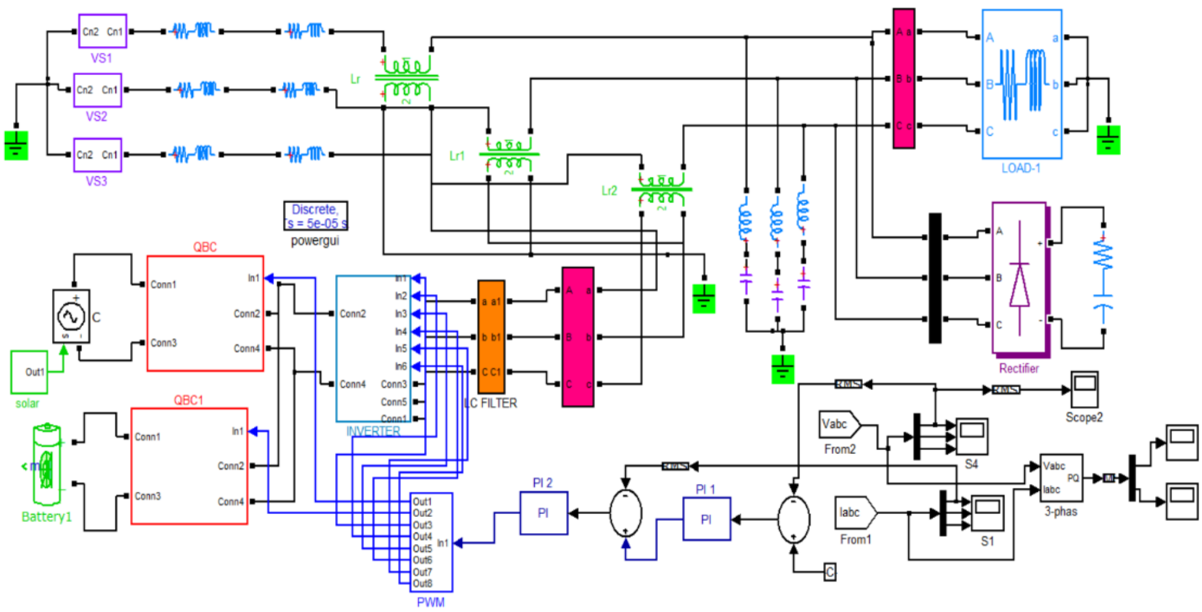

Figure 6. System schematic of QBC-HAF using a PI controller

Table 1. The proposed QBC and HAF system simulation specifications

Parameter	Value	Parameter	Value
K_p	0.5	C_4	100 µF
K_I	1.5	L_4	50 mH
K_D	0.018	MOSFET (IRF840)	500 V/8 A
K_λ	1	Diode	230 V/1 A
C_1	500 µF	Load resistance (R_0)	200 Ω
L_1	5.0 mH	Switching frequency (fs)	5 KHz
C_2	10 µF	Sampling time	1 µs
L_2	1.5 mH	PV voltage	48 V
C_3	20 µF	Battery voltage	24 V
L_3	10 mH		

3.1.1. Output voltage of PI controller

The maximum voltage of the output is around 4600 V, as shown in Figure 7. This high voltage is a measure of the system's capability to operate at high voltage with stability of the system's waveform. The harmonic distortion is effectively minimized by the proposed QBC-HAF control strategy, as can be seen from the nearly sinusoidal profile. Furthermore, the waveform showcases the robust performance of the system in grid-connected applications, indicating its ability to provide enhanced power quality and reliability.

3.1.2. Output voltage THD of PI controller

The output voltage THD of the PI controller, illustrated in Figure 8, is around 4.75%. This level of distortion shows that the PI controller is capable of controlling the voltage well but does not completely remove the harmonic components from the system. The relatively higher THD points out the challenges of PI control and the need for more sophisticated control methods, like fractional-order controllers, to provide better harmonic reduction and superior power quality performance.

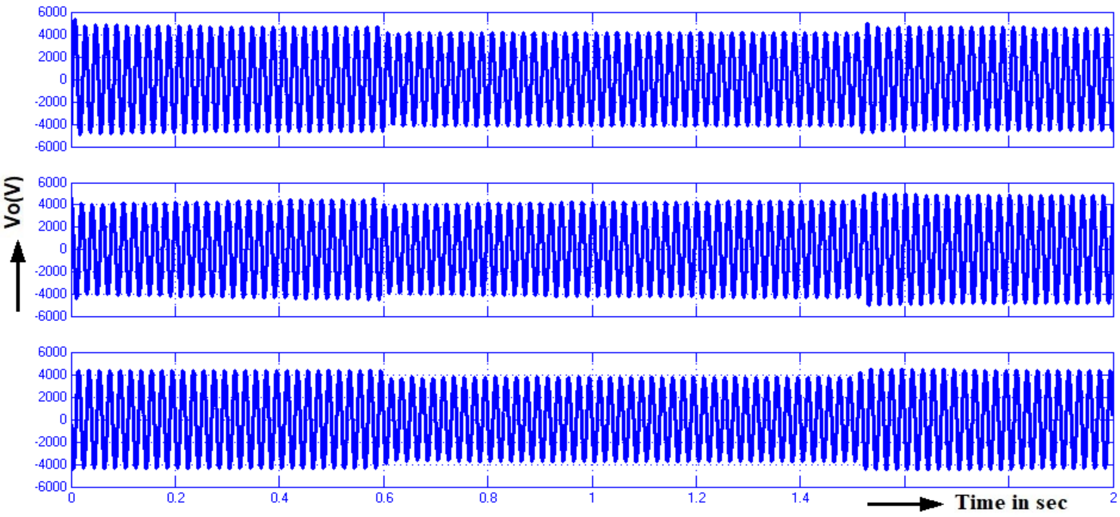

Figure 7. Output voltage of the PI controller

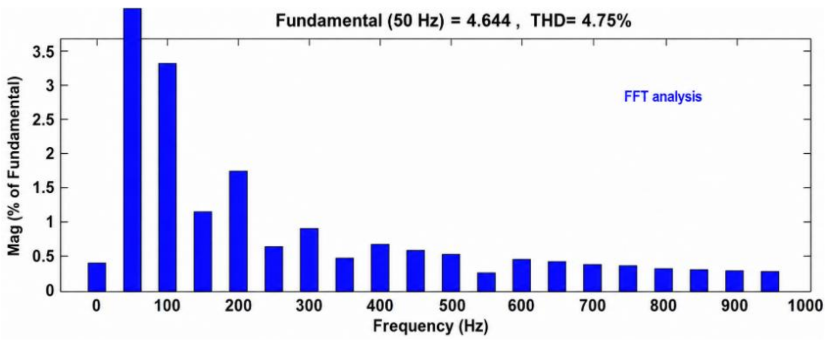

Figure 8. Output voltage THD of PI controller

3.1.3. Output current of PI controller

The output current waveform is illustrated in Figure 9 with the system operating in the PI mode, where an average load current of 13.2 A is supplied. The controller's performance remains consistent even under load, as evidenced by this steady current delivery. The waveform, however, also reveals some harmonic suppression limitations, and there is a need for more sophisticated control strategies to achieve better power quality.

3.1.4. Output current THD of PI controller

The THD of the output current is illustrated in Figure 10, which is around 4.34%. This proves the better waveform quality obtained with the hybrid active filter, demonstrating its capability to lower harmonic distortion from that of the conventional PI control. The lower THD value further highlights the ability of the proposed system to improve the overall power quality and enhance stability of operation in grid connected mode.

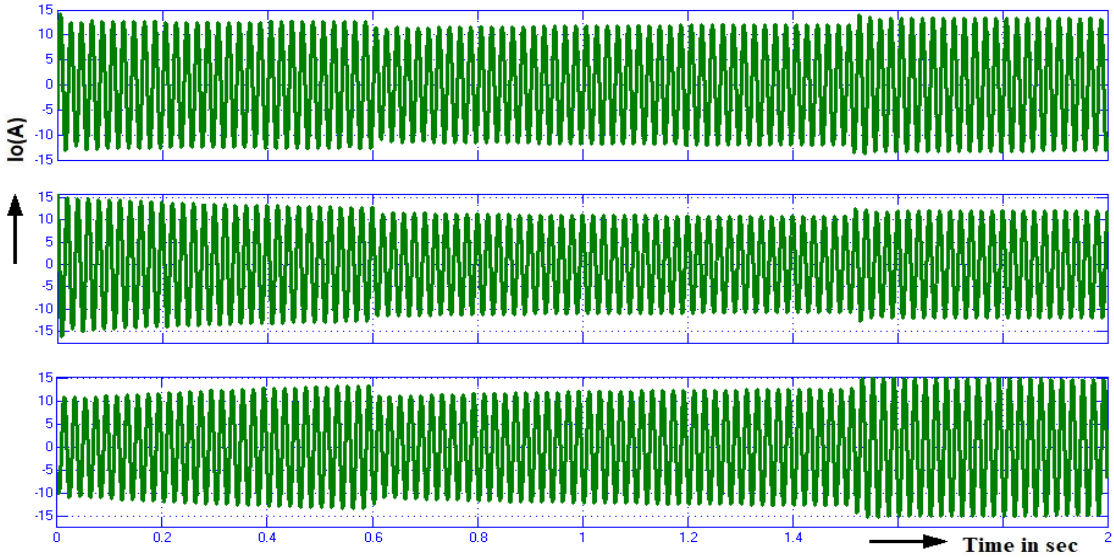

Figure 9. Output current of the PI controller

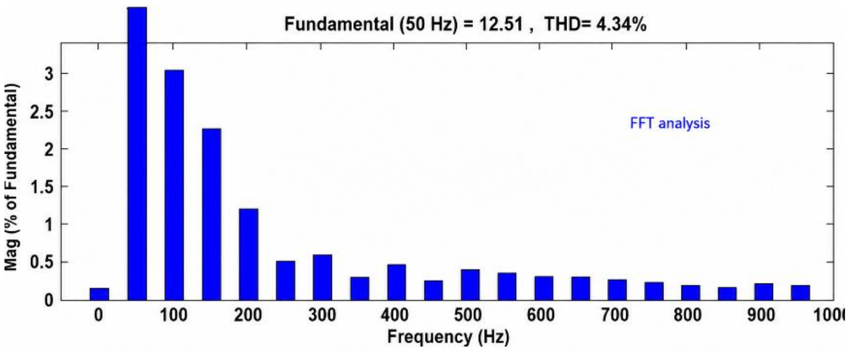

Figure 10. Output current THD of PI controller

3.1.5. Real power of PI controller

The real-power measurement of the PI controller, as depicted in Figure 11, indicates a delivered power of about 8.325 MW. This value reflects the controller's capability of properly controlling the active power flow, so that the system is able to supply the required load under steady-state conditions. Additionally, the measured output illustrates the drawbacks of traditional PI control, and while maintaining the real power output of this magnitude might be acceptable, it could still be associated with higher harmonic distortion; thus, the use of advanced control strategies becomes more compelling to increase the benefits of efficiency and overall power quality.

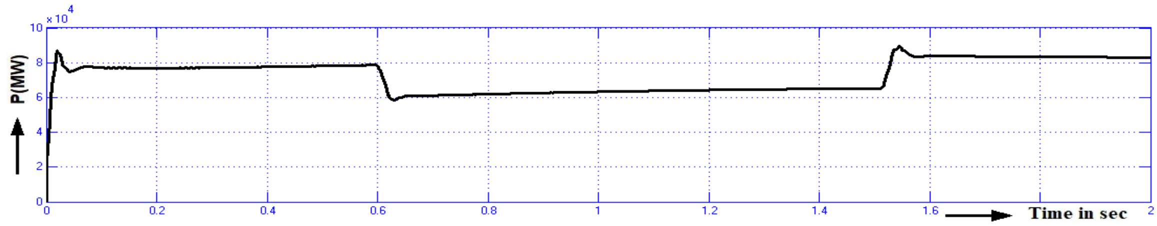

Figure 11. Real power of PI controller

3.1.6. Reactive power of PI controller

The reactive power profile shown in Figure 12 reveals that the reactive power is about 3.98 MVAR. These results indicate the converter's ability to control current and keep the power-quality indices within the acceptable range. Furthermore, the steady reactive-power response shows the efficiency of the proposed QBC-HAF configuration in dynamically responding to the reactive demand, enhancing the voltage stability, and reducing stress on the grid components.

3.2. System schematic of QBC-HAF using FOPID controller using MATLAB/Simulink

Figure 13 shows the QBC system coupled with the HAF that is regulated through a closed-loop FOPID control strategy. Using fractional-order control improves system response time so that it is able to reach and maintain steady-state values with greater accuracy in comparison to a traditional PI controller. In addition, when using a FOPID controller, the transient behavior of volts-over-frequencies operating characteristics can be shaped in a more flexible way in order to ensure voltage control while adjusting system operating conditions. This illustrates the flexibility that the QBC-HAF combination offers to enhance power quality and enhance system reliability in grid-connected applications.

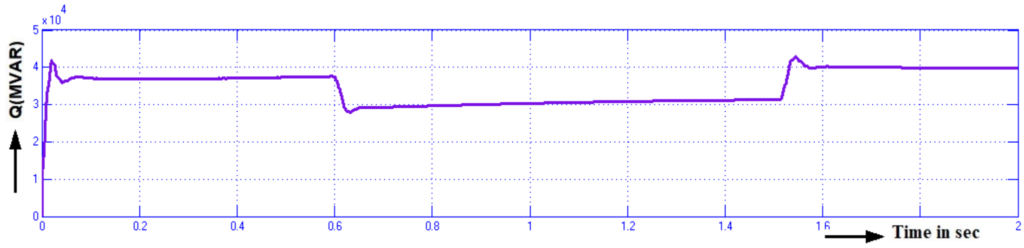

Figure 12. Reactive power of PI controller

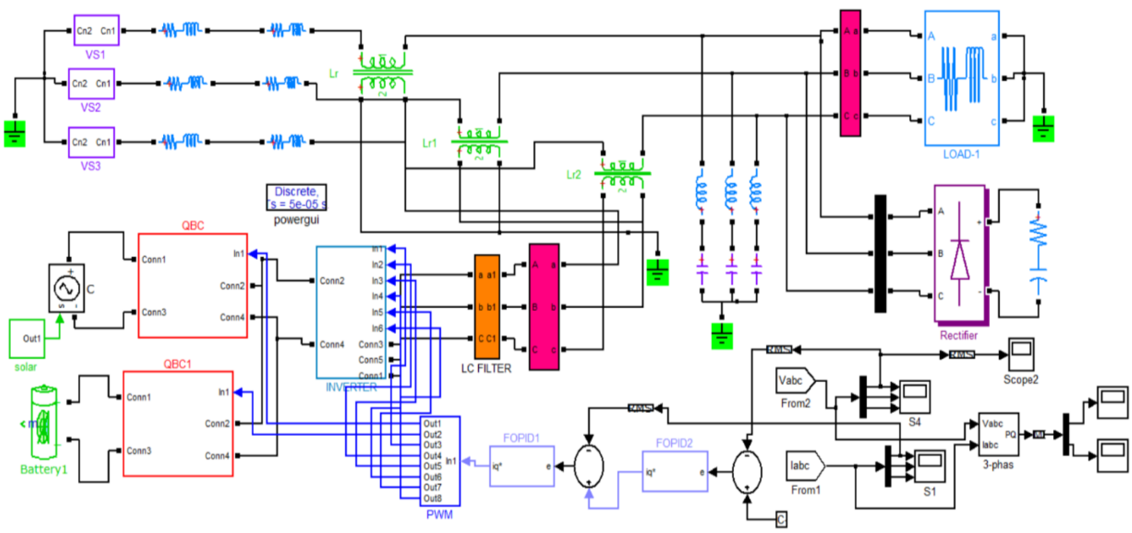

Figure 13. System schematic of QBC-HAF using FOPID controller

3.2.1. Output voltage of FOPID controller

The output voltage instantaneous waveform in Figure 14 indicates that the peak output voltage is about 4600 V. This high voltage level shows the system's capability to run at a high level with stable waveforms. The profile is close to sinusoidal, which further reinforces the effectiveness of harmonic suppression, thus proving the effectiveness of the proposed QBC-HAF control strategy.

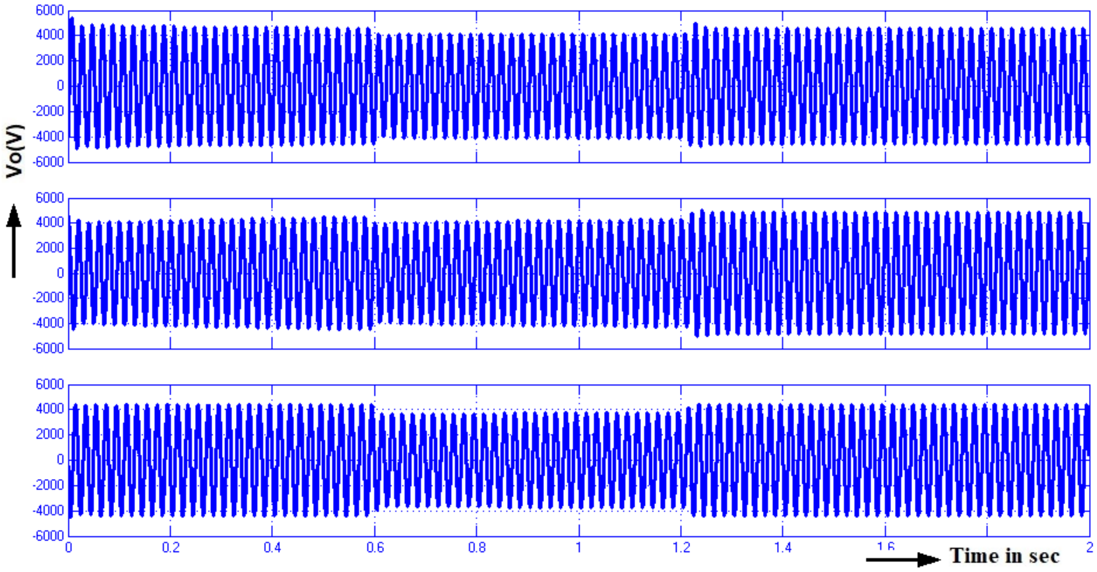

Figure 14. Output voltage of the FOPID controller

3.2.2. Spectral evaluation of the output voltage before mitigation using the FOPID controller

Before using the FOPID controller, the output voltage was analyzed spectrally, and the THD is shown in Figure 15 as 9.22%. This high distortion level reveals the high level of harmonics present in the system before filtering. The outcome gives a baseline condition on which the effectiveness of the harmonic suppression by the proposed hybrid active filter can be compared.

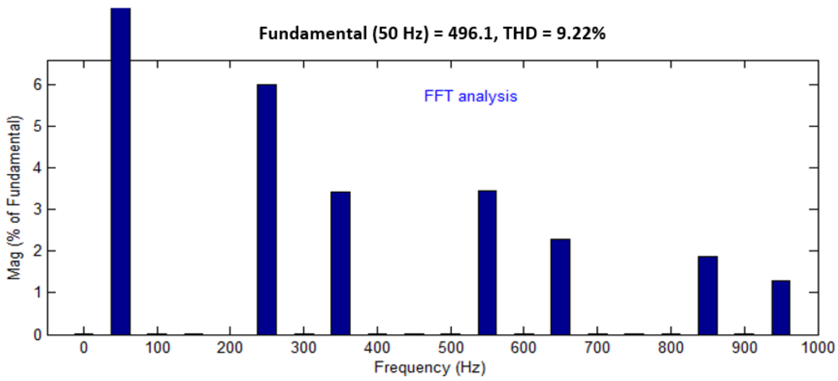

Figure 15. Spectral evaluation of the output voltage before mitigation

3.2.3. Spectral evaluation of the output voltage after mitigation using the FOPID controller

Figure 16 illustrates the spectral evaluation of the output voltage after mitigation using the FOPID controller. The output voltage THD is minimized from 9.22% before mitigation to 4.42% after mitigation, demonstrating the effectiveness of the proposed mitigation technique. The output current waveform, illustrated in Figure 17, indicates that the system supplies an average load current of approximately 13.2 A under FOPID-controlled operation.

3.2.4. Output current of FOPID controller

Figure 17 shows the output current waveform for the average load current at around 13.2 A under FOPID control. The constant delivery of this current by the controller demonstrates its performance consistency and the improvement of the waveform quality. Better waveform quality as a result of FOPID control further validates the improvement of power quality.

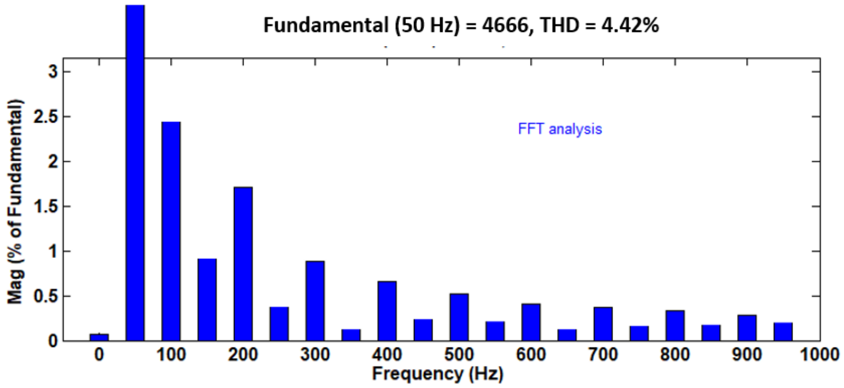

Figure 16. Spectral evaluation of the output voltage after mitigation

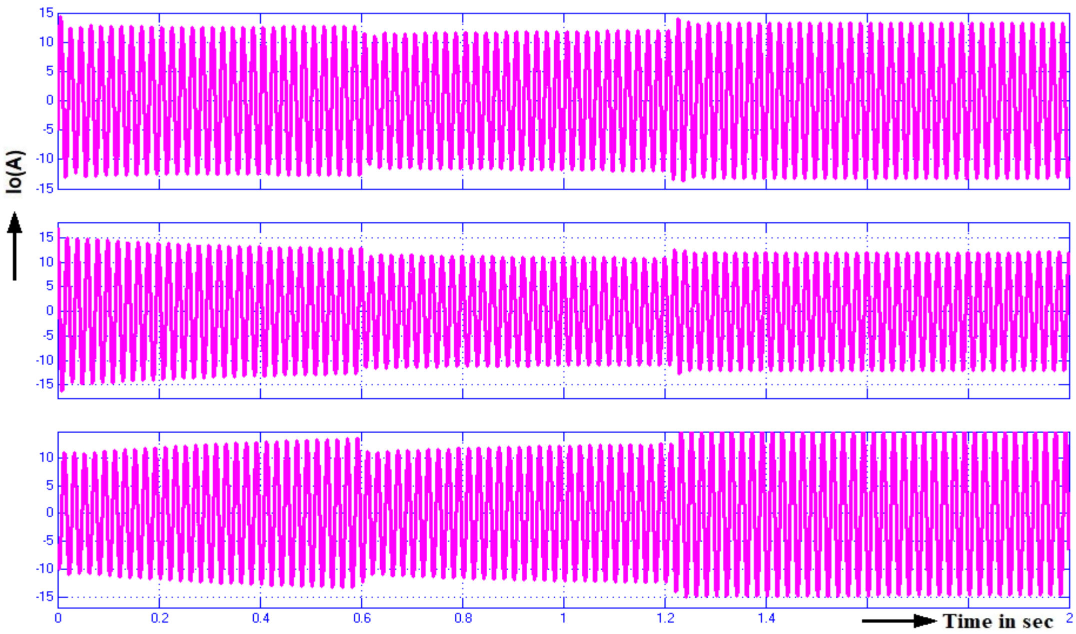

Figure 17. Output current of FOPID controller

3.2.5. Spectral evaluation of the output current before mitigation using the FOPID controller

Figure 18 displays an analysis of output current distortion spectral data before filter implementation. Based on the FOPID controller, THD is 10.13%. Without a filter, the system contains a dominant harmonic. This result will help assess the performance of the proposed hybrid active filter for the reduction of harmonic current.

3.2.6. Spectral evaluation of the output current after mitigation using the FOPID controller

Figure 19 demonstrates the spectral evaluation of the output current after mitigation using the FOPID controller. The output current THD is reduced from 10.13% before mitigation to 4.14% after mitigation, demonstrating the effectiveness of the proposed compensation technique. Table 2 presents the comparison of spectral evaluation between before and after output-voltage and output current THD for the QBC equipped with a HAF using FOPID controllers.

3.2.7. Real power of FOPID controller

Figure 20 illustrates the real power measurement of the FOPID controller with a delivered power of about 8.25 MW, while the reactive power of the FOPID controller profile is illustrated in Figure 21, which records a value close to 3.98 MVAR. These results demonstrate enhanced current regulation, reduced distortion, and improved power-quality performance with the FOPID controller.

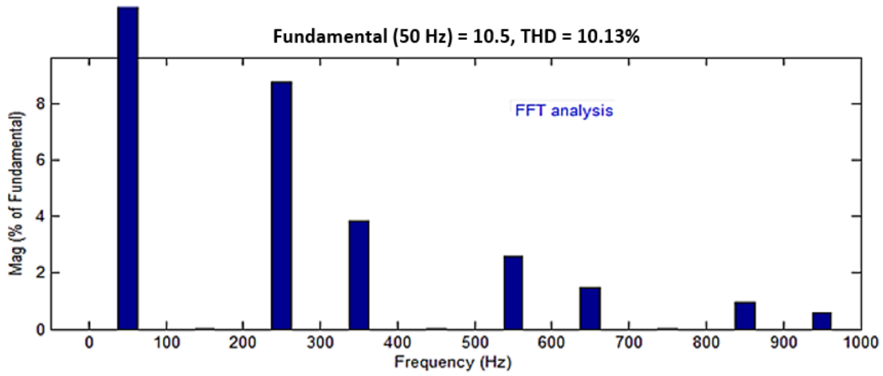

Figure 18. Spectral evaluation of the output current before mitigation

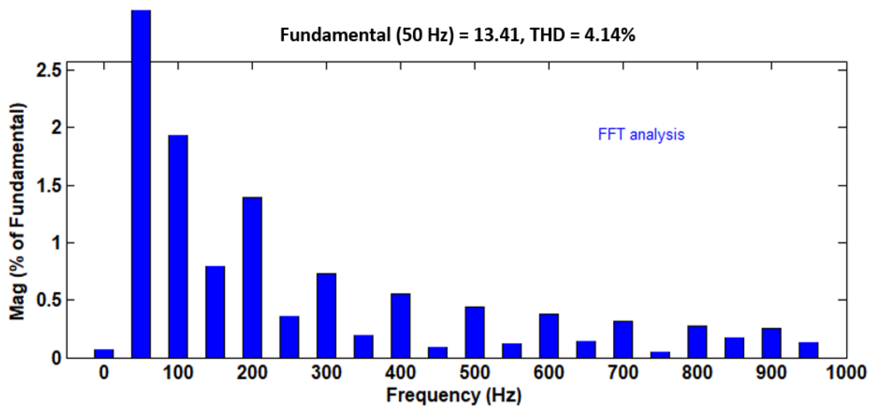

Figure 19. Spectral evaluation of the output current after mitigation

Table 2. Comparison of spectral evaluation between before and after output voltage and output-current THD

FFT evaluation	Output voltage THD (%)	Output current THD (%)
Before mitigation	9.22	10.13
After mitigation	4.42	4.14

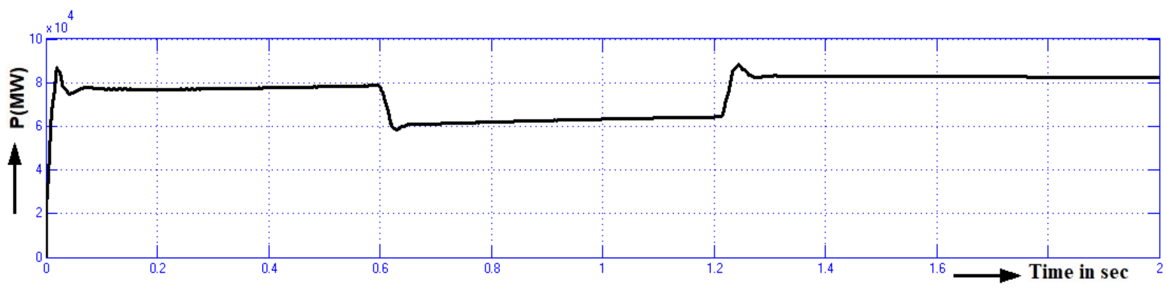

Figure 20. Real power of the FOPID controller

3.2.8. Reactive power of the FOPID controller

The transient response parameters of the PI and FOPID controllers were summarized in Table 3. The PI controller has slower dynamics, with rising values of the transient response Tr = 1.52 s, Tp = 1.54 s, and Ts = 1.55 s, and a large steady-state error of 2.73, while the FOPID controller has faster dynamics with the transient response Tr = 1.23 s, Tp = 1.24 s, and Ts = 1.26 s, and a smaller steady-state error of 2.15. From these results, the stability and the overall power quality of the system using the FOPID controller are proven to be better than the conventional PI controller, which provides better speed and accuracy.

Table 4 shows the performance of the PI and FOPID controllers with respect to harmonic distortion. The result shows that the output current THD for the PI controller is 4.34%, the output voltage THD for the PI controller is 4.75%, while the FOPID controller has a lower output current THD of 4.14% and output voltage THD of 4.42%. The results validate the superior performance of the FOPID controller in harmonic suppression compared to the conventional PI controller, thereby improving the quality of the power supply waveform and hence improving the overall power quality in grid-connected mode.

Table 5 shows the comparison of the performance of PI and FOPID controllers in terms of peak overshoot voltage and error indices. The PI controller has 2.72% overshoot, integral absolute error of 1.86, and integral square error of 0.83. The FOPID controller, on the other hand, has a lower overshoot of 1.95% and much lower error values of 1.25 and 0.49, making it more precise and efficient. The results demonstrate the efficiency of FOPID control for reducing the overshoot and the error metrics, which leads to better dynamic response and reliability of the system than conventional PI control.

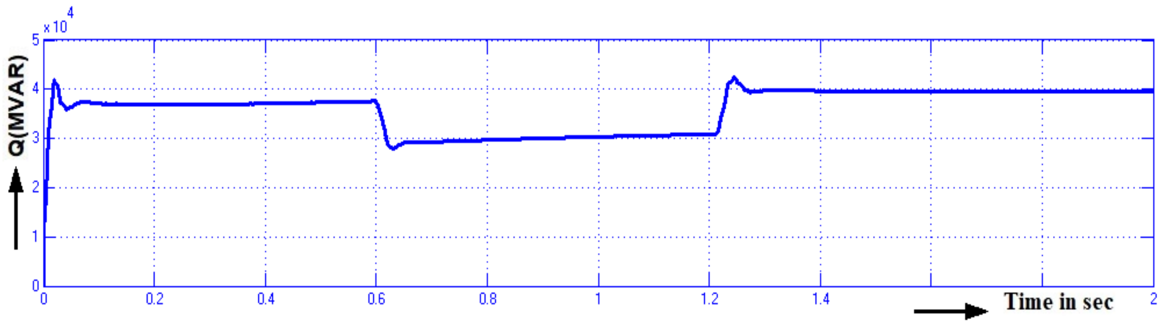

Figure 21. Reactive power of FOPID controller

Table 3. Comparative evaluation of time-domain performance parameters

Controller	Tr	Tp	Ts	Ess
PI	1.52	1.54	1.55	2.73
FOPID	1.23	1.24	1.26	2.15

Table 4. Comparative evaluation of output current and voltage THD under PI and FOPID control

Controller	Current THD (%)	Voltage THD (%)
PI	4.34	4.75
FOPID	4.14	4.42

Table 5. Comparison of peak overshoot voltage and integral error criteria for the proposed system

Controller	Peak overshoot voltage (%)	Integral absolute error	Integral square error
PI	2.72	1.86	0.83
FOPID	1.95	1.25	0.49

4. PROTOTYPE HARDWARE ARRANGEMENT

Figure 22 shows the prototype configuration of the QBC hybrid active filter. The hardware of the QBC-HAF-RL load consists of a PV panel, battery rectifier board, Control circuit board, QBC 1 and QBC 2 circuit boards, and a three-phase inverter board. The duty cycle of the QBC and VSI is adjusted using a PIC16F84A. The pulses generated by the PIC16F84A are amplified using an IR2110 isolated board. The prototype output waveforms are presented in Figure 23 (see Appendix). Figure 23(a) shows the PV and battery input voltages applied to the control circuit, while Figure 23(b) shows the voltage across the QBC. Figure 23(c) presents the switching signals of inverter switches M1 and M3, and Figure 23(d) shows the switching signals of inverter switches M2 and M4. Figure 23(e) illustrates the output voltage across the hybrid active filter, while Figure 23(f) shows the output current through the RL load.

The experimental prototype employs a PIC16F84A microcontroller operating at a switching frequency of 5 kHz for generating PWM pulses. The gate signals are isolated and amplified using IR2110 gate-driver circuits before being applied to the MOSFET switches (IRF840). Voltage and current measurements are acquired using Hall-effect voltage and current sensors and observed using a digital storage oscilloscope. Electrolytic capacitors, ferrite-core inductors, PN junction diodes (IN4007), and PCB-based converter modules are used in the implementation. The detailed hardware specifications are recapped in Table 6. Table 6 presents the hardware specifications of the proposed QBC and HAF system integrated with HAF using PI and FOPID controllers.

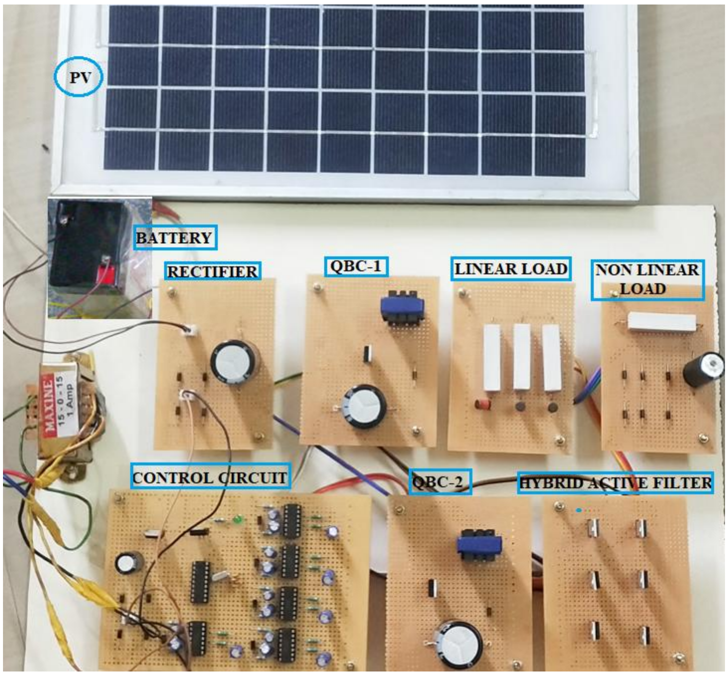

Figure 22. Prototype configuration of the hybrid active filter

Table 6. Hardware specifications of the proposed QBC and HAF system

S. No.	Name	Rating	Type	S. No.	Name	Rating	Type
1	Capacitor	1000 µF/25 V	Electrolytic	9	Resistor	100 E	Quarter watts
2	Capacitor	47 µF/63 V	Electrolytic	10	Resistor	22 E	Quarter watts
3	Capacitor	104 pF, 33 pF	disc	11	Regulator	12 V	L7812/TO3
4	Capacitor	2200 µF/63 V	Electrolytic	12	Regulator	5 V	L7805/TO220
5	Diode	IN4007-1000 V, 3 A	PN Junction	13	IC	IR2110	Opto-coupler
6	Inductance	1.5 µH	ferrite coil	14	Pic controller	PIC16F84A	RISC
7	MOSFET (IRF840)	500 V, 8 A	N-channel	15	PCB	V105	General
8	Frequency	5 kHz					

5. LIMITATIONS AND FUTURE SCOPE

The present work is validated through MATLAB/Simulink simulations and a laboratory-scale prototype under nominal conditions. Factors such as irradiance variation, battery aging, and large grid disturbances were not considered. Future extensions include applying model predictive control (MPC) for comparison with PI and FOPID controllers in the two-loop QBC–HAF system, and automatic tuning of FOPID parameters using optimization methods like particle swarm or jellyfish search. Implementation on FPGA/DSP platforms, scaling to higher power ratings, three-phase operation, and integration with other renewable sources such as wind are also promising directions. Further studies could examine performance under grid faults, unbalanced loads, EV charging, and microgrid applications, with machine learning–based adaptive control to enhance robustness and self-adjusting capability in real-world scenarios.

5.1. Sensitivity analysis of the proposed approach

The proposed controller maintains satisfactory voltage regulation under variations in solar irradiance, battery state of charge, and nonlinear load disturbances. This demonstrates its robustness in handling diverse operating conditions while ensuring stable system performance. Future work will include comprehensive sensitivity analysis under rapidly changing renewable energy inputs and grid disturbances, which will help evaluate the adaptability and resilience of the control strategy in real-world scenarios.

6. CONCLUSION

This paper presented a QBC with an HAF that integrates the design, analysis, simulations, and real experimental validations to refine the power quality of renewable energy-based grid-connected systems. The proposed system was studied using proportional integral (PI) and FOPID controllers to appraise their roles in tuning the harmonics and assessing the dynamic response. FOPID controller was verified with better results than the traditional PI controller. Current THD was brought down from 4.34% to 4.14%, while the THD of output voltage decreased from 4.75% to 4.42%. Additionally, the rise time, maximum time, and steady-state time of the response decreased from 1.52 s, 1.54 s, and 1.55 s to 1.23 s, 1.24 s, and 1.26 s, respectively. A reduction of 2.73 to 2.15 was also noted in the steady-state error, indicating a better dynamic response and control of the system. Validation of the developed QBC–HAF experimental setup was done using the FOPID controller, and results showed that it had better harmonic and power quality and dynamic response. Further, the integrated renewable energy system was validated for power electronic applications. The present work deals with investigations on a FOPID-controlled two-loop QBC-HAF system. The investigations on model-predictive controlled two-loop QBC-HAF systems will be done in the future.

According to IEEE Standard 519-2022, the current THD at the point of common coupling should generally remain below 5% for low-voltage systems. The proposed FOPID-controlled QBC–HAF system achieves a current THD of 4.14% and a voltage THD of 4.42%, satisfying the recommended harmonic limits and demonstrating compliance with IEEE 519.

ACKNOWLEDGEMENT

This work was supported by Hindustan Institute of Technology and Science.

FUNDING INFORMATION

Authors state no funding involved.

AUTHOR CONTRIBUTIONS STATEMENT

This journal uses the Contributor Roles Taxonomy (CRediT) to recognize individual author contributions, reduce authorship disputes, and facilitate collaboration.

Name of Author	C	M	So	Va	Fo	I	R	D	O	E	Vi	Su	P	Fu
S. Venkata Ramana Rao	✓	✓	✓	✓	✓	✓		✓	✓	✓	✓		✓	
Mahiban Lindsay		✓		✓		✓	✓	✓	✓	✓	✓	✓	✓	

C : **C**onceptualization
M : **M**ethodology
So : **So**ftware
Va : **Va**lidation
Fo : **Fo**rmal analysis
I : **I**nvestigation
R : **R**esources
D : **D**ata Curation
O : Writing - **O**riginal Draft
E : Writing - Review & **E**diting
Vi : **Vi**sualization
Su : **Su**pervision
P : **P**roject administration
Fu : **Fu**nding acquisition

CONFLICT OF INTEREST STATEMENT

Authors state no conflict of interest.

DATA AVAILABILITY

Data availability is not applicable to this paper as no new data were created or analyzed in this study.

REFERENCES

[1] B. Adel, M. Tarek, and K. Samia, "Mitigating harmonic distortion in grid-connected PV systems: a comparative evaluation of ANFIS and IC-based MPPT techniques," *International Journal of Power Electronics and Drive Systems (IJPEDS)*, vol. 17, no. 1, p. 303, Mar. 2026, doi: 10.11591/ijpeds.v17.i1.pp303-316.

[2] A. Gholami, M. Ameri, M. Zandi, R. G. Ghoachani, S. Eslami, and S. Pierfederici, "Photovoltaic potential assessment and dust impacts on photovoltaic systems in Iran: review paper," *IEEE Journal of Photovoltaics*, vol. 10, no. 3, pp. 824–837, May 2020, doi: 10.1109/JPHOTOV.2020.2978851.

[3] A. M. Adeyinka, O. C. Esan, A. O. Ijaola, and P. K. Farayibi, "Advancements in hybrid energy storage systems for enhancing renewable energy-to-grid integration," *Sustainable Energy Research*, vol. 11, no. 1, p. 26, Jul. 2024, doi: 10.1186/s40807-024-00120-4.

[4] A. Daghouri, S. El Hani, Y. El Hachimi, and H. Mediouni, "Enhanced hybrid energy storage system combining battery and supercapacitor to extend nanosatellite lifespan," *Results in Engineering*, vol. 23, 2024, doi: 10.1016/j.rineng.2024.102634.

[5] S. K. Ojha, C. O. Maddela, and L. N. Chanu, "A novel fractional order controller for stability enhancement of renewable energy integrated multi area power system with hybrid energy storage," *Scientific Reports*, vol. 16, no. 1, p. 21577, May 2026, doi: 10.1038/s41598-026-50496-0.

[6] H. Manoharan, S. Karuppannan, K. Chandrasekaran, and S. Barua, "Power quality improvement of grid-connected solar power plant systems using a novel fractional order proportional integral derivative controller technique," *IET Renewable Power Generation*, vol. 18, no. 15, pp. 3268–3284, Nov. 2024, doi: 10.1049/rpg2.13128.

[7] H. A. Issa, L. M. Abdali, H. Alhusseini, and V. I. Velkin, "Design, modeling, and control of a dual-axis solar tracker using fractional order PID controllers for enhanced energy efficiency," *Results in Engineering*, vol. 27, p. 106073, Sep. 2025, doi: 10.1016/j.rineng.2025.106073.

[8] N. K. Pandey, R. K. Pachauri, S. Choudhary, and A. F. Minai, "Power quality improvement using rabbit optimization FOPID controlled photovoltaic- battery powered hybrid power filter," *Renewable Energy Focus*, vol. 47, p. 100508, Dec. 2023, doi: 10.1016/j.ref.2023.100508.

[9] K. N. Khallouf, H. Benbouhenni, and N. Bizon, "Advancing sustainable energy management in hybrid power systems via a novel nonlinear approach employing fractional-order PI controllers," *Sustainability*, vol. 18, no. 10, p. 5025, May 2026, doi: 10.3390/su18105025.

[10] K. K. Gupta and P. Bhatnagar, *Multilevel inverters: Conventional and emerging topologies and their control*. Elsevier, 2017. doi: 10.1016/C2016-0-03360-0.

[11] F. Elghabsi *et al.*, "High gain and high efficiency soft switching quadratic boost converter for renewable energy applications," *Scientific Reports*, vol. 15, no. 1, p. 36238, Oct. 2025, doi: 10.1038/s41598-025-20207-2.

[12] S. Pinninti and S. R. Sura, "An optimal demand side management for microgrid cost minimization considering renewables," *Optimal Control Applications and Methods*, vol. 46, no. 1, pp. 197–214, Jan. 2025, doi: 10.1002/oca.3205.

[13] S. Etedali, A.-A. Zamani, M. Akbari, and M. Seifi, "A new seismic control framework of optimal PIλDμ controller series with fuzzy PD controller including soil-structure interaction," *Journal of the Franklin Institute*, vol. 360, no. 14, pp. 10536–10563, Sep. 2023, doi: 10.1016/j.jfranklin.2023.08.003.

[14] J. Jayaudhaya, T. Magesh, G. Devi, L. A. Isabella, and R. Thangavelu, "Optimal control of FOPID controllers for PMSG wind energy conversion system using golden eagle optimization algorithm," *Electrical Engineering*, vol. 107, no. 11, pp. 14655–14670, Nov. 2025, doi: 10.1007/s00202-025-03285-3.

[15] B. B. Taya, A. Ahammad, and F. I. Jahin, "Total harmonic distortion mitigation and voltage control using distribution static synchronous compensator and hybrid active power filter," *International Journal of Advanced Technology and Engineering Exploration*, vol. 11, no. 114, May 2024, doi: 10.19101/IJATEE.2023.10102587.

[16] W. Ahamd and I. Ullah, "unified power quality conditioner based power quality improvement in micro-grid," in *2025 IEEE Texas Power and Energy Conference (TPEC)*, IEEE, Feb. 2025, pp. 1–6. doi: 10.1109/TPEC63981.2025.10906828.

[17] O. K. Al Basri, F. K. Nori, and M. A. Hussein, "Enhanced power quality in grid-connected photovoltaic systems using a novel modular multilevel inverter topology," *Journal of Renewable Energy and Environment (JREE)*, vol. 12, no. 4, pp. 102–113, 2025, doi: 10.30501/jree.2025.534417.2496.

[18] S. Shi, D. Liu, and J. Han, "Small signal modeling and performance analysis of conventional- and dual-UPQC," *IEEE Access*, vol. 12, pp. 11909–11925, 2024, doi: 10.1109/ACCESS.2024.3355590.

[19] A. Amirullah and A. Adiananda, "Dual fuzzy-Sugeno method to enhance power quality performance using a single-phase dual UPQC-dual PV without DC-link capacitor," *Protection and Control of Modern Power Systems*, vol. 9, no. 1, pp. 133–153, Jan. 2024, doi: 10.23919/PCMP.2023.000107.

[20] C. D. Sanjenbam and B. Singh, "Power quality enhancement of standalone hydropower generation system through modified integrator based observer controlled UPQC," *Electric Power Systems Research*, vol. 226, p. 109941, Jan. 2024, doi: 10.1016/j.epsr.2023.109941.

[21] A. Hirsch, Y. Parag, and J. Guerrero, "Microgrids: A review of technologies, key drivers, and outstanding issues," *Renewable and Sustainable Energy Reviews*, vol. 90, pp. 402–411, Jul. 2018, doi: 10.1016/j.rser.2018.03.040.

[22] M. Golla, S. Sankar, and K. Chandrasekaran, "Renewable integrated UAPF fed microgrid system for power quality enhancement and effective power flow management," *International Journal of Electrical Power & Energy Systems*, vol. 133, p. 107301, Dec. 2021, doi: 10.1016/j.ijepes.2021.107301.

[23] M. L. Aganović, T. Konjić, M. Milovanović, M. Ćalasan, A. I. Omar, and S. H. E. Abdel Aleem, "Power quality in modern power systems: a case study in Bosnia and Herzegovina," in *Modernization of Electric Power Systems*, Cham: Springer International Publishing, 2023, pp. 181–204. doi: 10.1007/978-3-031-18996-8_7.

[24] S. S. Dheeban and N. B. Muthu Selvan, "ANFIS-based power quality improvement by photovoltaic integrated UPQC at distribution system," *IETE Journal of Research*, vol. 69, no. 5, pp. 2353–2371, Jul. 2023, doi: 10.1080/03772063.2021.1888325.

[25] A. Aldosary, "Power quality conditioners-based fractional-order PID controllers using hybrid jellyfish search and particle swarm algorithm for power quality enhancement," *Fractal and Fractional*, vol. 8, no. 3, p. 140, Feb. 2024, doi: 10.3390/fractalfract8030140.

APPENDIX

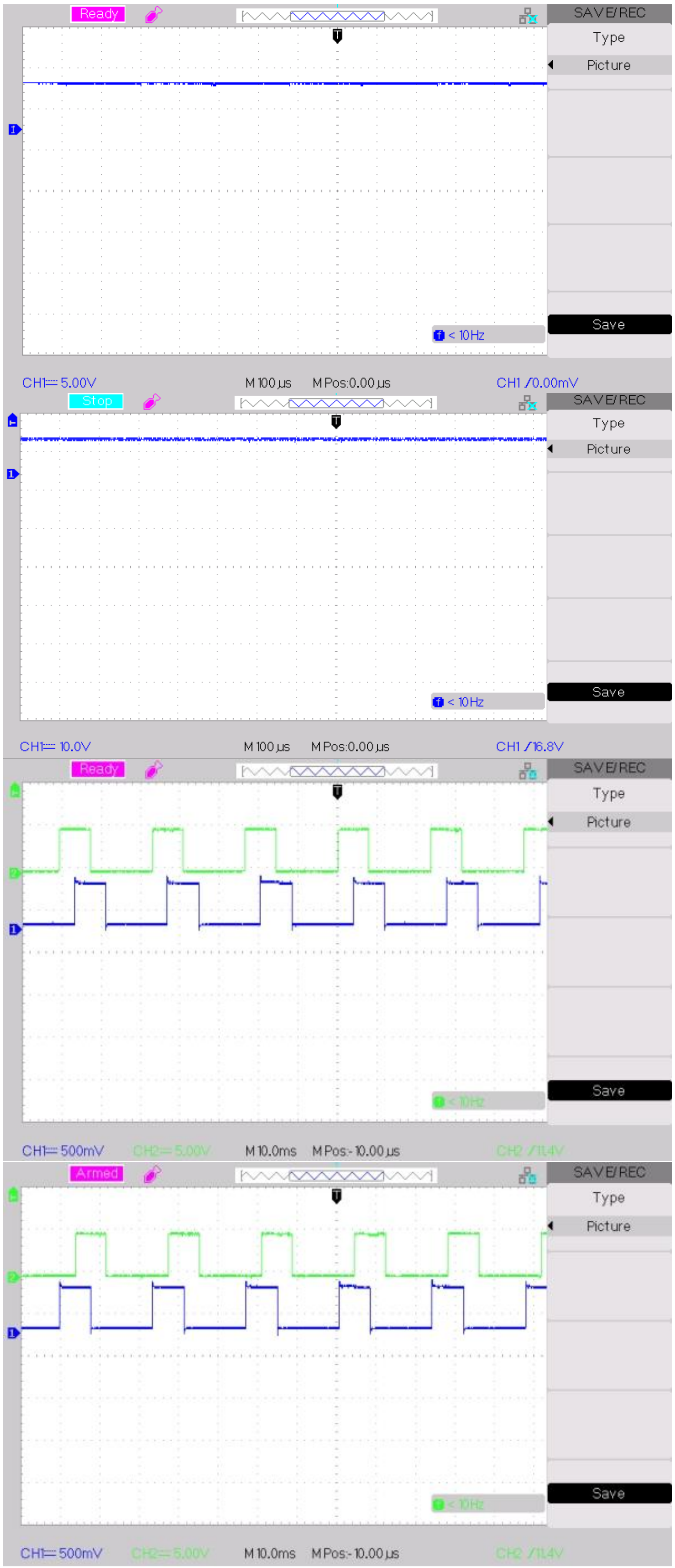

(a)

(b)

(c)

(d)

Figure 23. Prototype output waveform: (a) input voltage across PV and battery, (b) voltage across QBC, (c) switching signals of inverter switches M1 and M3, and (d) switching signals of inverter switches M2 and M4

(e)

(f)

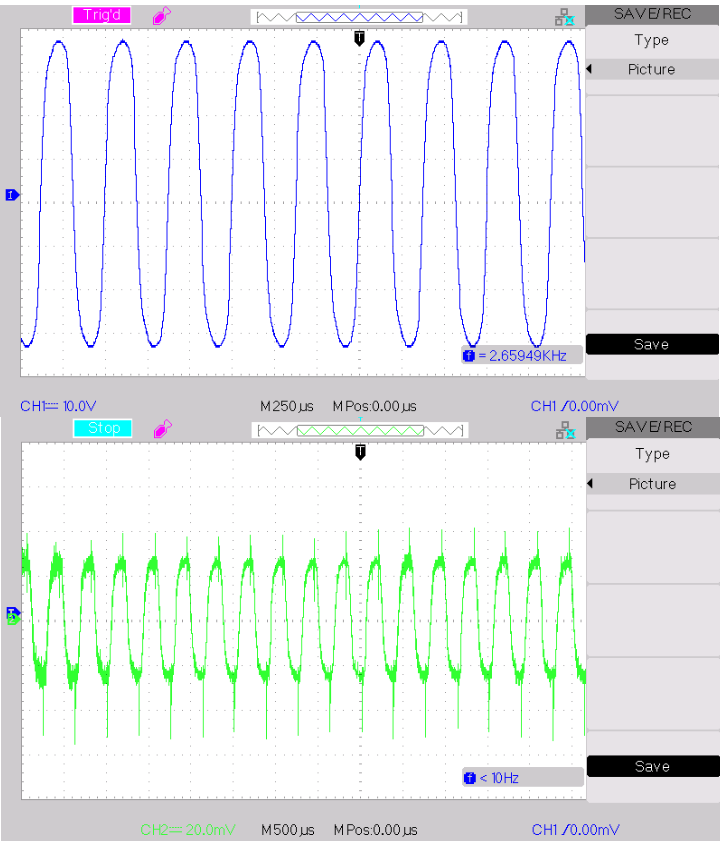

Figure 23. Prototype output waveform: (e) output voltage across the hybrid active filter and (f) output current through RL load (continued)

BIOGRAPHIES OF AUTHORS

S. Venkata Ramana Rao is an assistant professor in the Department of Electrical and Electronics Engineering at H.I.T.S., Chennai, India. He received his B.Eng. and M.Eng. degrees in electrical and electronics engineering from Tagore Engineering College and Sathyabama College, Chennai, India, in 2009 and 2015, respectively. He has been serving as an assistant professor at H.I.T.S., Chennai, since 2024. His research interests include digital electronics, power systems, IoT, industrial informatics, power electronics, renewable energy, FPGA applications, embedded systems, artificial intelligence, intelligent control, and digital libraries. He can be contacted at email: vramanor@hindustanuniv.ac.in.

Dr. Mahiban Lindsay received his Ph.D. in power system reliability from Hindustan University, Chennai. He received his M.E. degree in power system engineering and B.E. degree in electrical and electronics engineering from Anna University. He is a recipient of the Gold Medal in his master's in power system engineering from Anna University. Currently, he is serving as a professor and Head of the Department of Electrical and Electronics Engineering. He has also served as a visiting faculty member at Anna University. He has coordinated international corporate training programs and delivered various engineering topics to industrial professionals in India and abroad. His major teaching areas include power systems, control systems, and electrical machines. He has published several articles in journals and conference proceedings. He can be contacted at email: nmlindsay@hindustanuniv.ac.in.